Ceramics International xxx (xxxx) xxx

Contents lists available at ScienceDirect

Ceramics International

journal homepage: www.elsevier.com/locate/ceramint

Phosphate source induced rapid synthesis of urchin-like hydrated $GdPO_4$: Eu^{3+} nanoparticles: Imaging and drug delivery in A549 cell line

Ganji Lakshmi Varaprasad [a], Hoomin Lee [a], Suheon Kim [a], Eunsu Kim [a], Eluri Pavitra [a], Neeraja Valluru [b], Young-Kyu Han [c], Ganji Seeta Rama Raju [c,*], Yun Suk Huh [a,**]

[a] Department of Biological Engineering, Biohybrid Systems Research Center (BSRC), Inha University, Incheon, 22212, Republic of Korea
[b] SWR Government Degree College (Affiliated to Krishna University), Kanchikacherla, Vijayawada, Andhra Pradesh, 52004, India
[c] Department of Energy and Materials Engineering, Dongguk University, Seoul, 04620, Republic of Korea

ARTICLE INFO

Keywords:
Urchin-like morphology
Photoluminescence
A549 cells
Bioimaging
Drug delivery

ABSTRACT

Energy and environmental concerns are increasing owing to the increased consumption of resources. To help solve the energy crisis and contribute to protecting our environment, this study aimed to develop a fast and eco-friendly method of synthesis. We propose a H_3PO_4 assisted fast synthesis technique for developing urchin-like $GdPO_4{\cdot}xH_2O{:}5Eu^{3+}$ nanoparticles. First, $Gd(OH)CO_3{:}5Eu^{3+}$ nanospheres with sizes of about 60 nm were developed using urea-based homogeneous precipitation. These nanospheres were utilized as the Gd^{3+} source and sacrificial templates in the formation of urchin-like $GdPO_4.xH_2O{:}5Eu^{3+}$ nanoparticles, where the Kirkendall effect takes place during hydrothermal synthesis. The structural properties confirmed the existence of the H_2O phase in the $GdPO_4{:}5Eu^{3+}$ nanoparticles. The synthesized urchin-like $GdPO4{\cdot}xH_2O{:}5Eu^{3+}$ nanoparticles exhibited excellent photoluminescence in the reddish-orange region upon excitation by near-UV excitation wavelengths. These urchin-like nanoparticles demonstrated effective penetration in lung cancer cells by exhibiting luminescence from both the cytoplasm and nucleoplasm. The conjugation of doxorubicin with urchin-like $GdPO_4{\cdot}xH_2O{:}5Eu^{3+}$ nanoparticles helped to realize efficient antitumor activity against lung cancer.

1. Introduction

In recent years, considerable progress has been made in the field of nanotechnology by designing and improving the characteristics of novel multifunctional inorganic nanoparticles, which can contribute to almost every field of science [1]. In the biomedical field, owing to their unique characteristics, including superior biocompatibility, high water dispersion, low toxicity, and controlled drug release [2,3], multifunctional nanoparticles provide a gateway to modify the pharmacokinetic profile of drugs compared to conventional therapeutic modalities. Recently, rare-earth orthophosphates ($REPO_4$) have been drawing a lot of attention in the biomedical field owing to their exceptional properties such as high quantum yield, excellent biocompatibility, low photo-bleaching potential, and high chemical and thermal stabilities [4,5]. Among several phosphate host matrices, gadolinium orthophosphate ($GdPO_4$) has been identified as one of the promising multifunctional nanoplatforms for various optoelectronic and biomedical applications [6,7]. Owing to their paramagnetic behavior, gadolinium-based host materials can be used to obtain more than one imaging modality, such as fluorescence imaging, optical imaging, ultrasound, and magnetic resonance imaging [8–10]. Therefore, a $GdPO_4$ host matrix doped with suitable rare-earth ions has captured the attention of researchers as a novel bifunctional host material for multimodal bioimaging and drug delivery applications.

To avoid the shortcomings of traditional core-shell nanostructures, nowadays, most research has focused on synthesizing hollow and/or mesoporous nanoparticles [11,12]. Traditional template-based routes are typically used for synthesizing hollow nanostructures, however, to reduce the cost, energy, and time-demands, several direct methods of synthesis have been developed with the aid of etching, Ostwald ripening, and Kirkendall effect, where external templating agents are not required [13,14]. The Kirkendall effect, also known as the self-templating approach, modifies the structure and shape of nanoparticles by interdiffusion and create hollow or urchin-like structures

* Corresponding author.
** Corresponding author.
E-mail addresses: gseetaramaraju7@dongguk.edu, gseetaramaraju@live.in (G.S.R. Raju), yunsuk.huh@inha.ac.kr (Y.S. Huh).

https://doi.org/10.1016/j.ceramint.2022.05.086
Received 7 March 2022; Received in revised form 23 April 2022; Accepted 7 May 2022
Available online 10 May 2022

[15,16]. Several studies have thus far investigated RE ion-doped $GdPO_4$ nanostructures with different morphologies. Xu et al. [7] and Zhang et al. [17] recently reported the preparation of urchin-like $GdPO_4$ hollow spheres by hydrothermal synthesis (180 °C for 24 h and 200 °C for 12 h, respectively). Li et al. [18] reported the synthesis of $GdPO_4$:Eu hollow spheres by etching (200 °C for 12 h), and Gao et al. [6] synthesized $GdPO_4$ hollow microspheres through a multistep transformation method using polystyrene spheres as the template (180 °C for 24 h followed by calcination at 800 °C for 4 h). All of these studies used $NH_4H_2PO_4$ as the phosphate source for synthesizing $GdPO_4$ hollow or urchin-like spheres.

To the best of our knowledge, no study has been performed on a $GdPO_4$ host material using phosphoric acid (H_3PO_4) as the phosphate source. Therefore, we aimed to synthesize $GdPO_4$:Eu^{3+} urchin-like nanospheres through a simple and energy-efficient process of hydrothermal synthesis (180 °C for 1 h) using H_3PO_4 as the phosphate source. First, tetrapropyl ammonium hydroxide (TPAOH)-assisted Gd(OH)CO_3:5Eu^{3+} nanospheres with the sizes of approximately 60 nm were synthesized. These nanospheres acted as the Gd source and sacrificial template during the formation of urchin-like $GdPO_4{\cdot}H_2O$:5Eu^{3+} nanoparticles. The observed structural properties confirmed their hydroxyl nature, and their photoluminescence (PL) properties resulted in excellent reddish-orange emission. Confocal microscopy imaging, drug (doxorubicin (DOX)) loading, and release efficiencies, coupled with cell viability studies, were performed to examine the potential of urchin-like $GdPO_4{\cdot}H_2O$:5Eu^{3+} nanoparticles for biomedical applications. Our results demonstrate that the synthesized urchin-like $GdPO_4{\cdot}H_2O$:5Eu^{3+} nanoparticles are cost-effective and also demonstrated excellent potential in future biomedical applications.

2. Experimental

2.1. Materials

Gadolinium nitrate hexahydrate [$Gd(NO_3)_3{\cdot}6H_2O$] (99.9%), europium nitrate pentahydrate [$Eu(NO_3)_3{\cdot}5H_2O$] (99.9%) were purchased from Sigma-Aldrich. TPAOH, phosphoric acid (H_3PO_4), urea [$CO(NH_2)_2$, 99–100.5%) were also purchased from Sigma-Aldrich. Deionized water (DI) (18.2 MΩ), from a Millipore Milli-Q system was used in all experiments. All chemical agents used in this experiment were of analytical grade and were used directly without further purification.

2.2. Synthesis of $Gd(OH)CO_3$:5Eu^{3+} colloidal nanospheres

Gd(OH)CO_3:Eu nanospheres as the precursor for the preparation of $GdPO_4$:5Eu^{3+} nanospheres were synthesized using a modified urea-based homogeneous precipitation method [19]. First, stoichiometric quantities of $Gd(NO_3)_3{\cdot}6H_2O$, $Eu(NO_3)_3{\cdot}5H_2O$, and urea (3 g) were dispersed in 100 ml of DI water. The mixture was vigorously stirred (500 rpm) using a magnetic stirrer at room temperature for 1 h until a homogenous solution was formed. TPAOH (20 µl) was added to reduce the size of the spheres. The homogenous mixture was then immersed in an oil bath and heated to 90 °C for 1 h, yielding white-colored monodispersed colloidal spheres of Gd(OH)CO_3:Eu^{3+} as a precipitate. The product was separated by centrifugation (5,000 rpm), followed by multiple washings with water and ethanol.

2.3. Synthesis of urchin-like $GdPO_4{\cdot}H_2O$:5Eu^{3+} nanoparticles

The as-prepared Gd(OH)CO_3:5Eu^{3+} nanospheres were dispersed in 40 ml DI water, sonicated for a few minutes (solution A), and then stirred for 30 min. Simultaneously, the calculated quantity of H_3PO_4 was dispersed in 30 ml of DI water and subject to magnetic stirring at 400 rpm for 30 min at room temperature (solution B). Solution A was then added dropwise to solution B with constant stirring at 400 rpm for 1 h. The mixed solution was subsequently transferred into a stainless-steel autoclave with a Teflon liner (120 ml with 60 % filling capacity), heated to 180 °C for 1 h, and left to cool to room temperature naturally. The white-colored precipitate was finally separated from the colloidal solution by centrifugation at 5,000 rpm, followed by multiple washings with copious volumes of DI water and ethanol to obtain urchin-like $GdPO_4{\cdot}H_2O$:5Eu^{3+} nanoparticles. To understand the growth process with respect to time, the same hydrothermal reaction was carried out at 180 °C for time periods ranging from 1 h to 24 h.

2.4. Cell cytotoxicity (CCK-8) assay

The cytotoxicity of urchin-like $GdPO_4{\cdot}H_2O$:5Eu^{3+} nanoparticles and the anti-cancer ability of $GdPO_4{\cdot}H_2O$:5Eu^{3+}@DOX were evaluated using the cell counting Kit-8 (CCK-8) assay. The percentage viability of lung cancer (A549) cell lines were calculated after culturing in Roswell Park Memorial Institute (RPMI) medium, where a medium containing 10% fetal bovine serum, 1% penicillin and streptomycin at 37 °C, and 5% CO_2 and harvested by trypsinization and subsequently seeded into a 96-well cell culture plate at 1×10^4 cells/well for 24 h. After seeding, cells were treated with urchin-like $GdPO_4{\cdot}H_2O$:5Eu^{3+} nanoparticles and incubated for 24 h. Cell viability was examined using a CCK-8 assay. Viability was assessed calorimetrically using a multi-reader (Varioskan LUX Multimode Microplate Reader) at an absorbance of 450 nm.

2.5. In vitro cell uptake assay

A549 cells (5×10^4) were seeded in a 6-well plate for 24 h. The cell lines were then treated with or without urchin-like $GdPO_4{\cdot}H_2O$:5Eu^{3+} nanoparticles. After 24 h of treatment, the cell lines were rinsed three times with 1x phosphate buffered saline (1x PBS) and incubated in 4% paraformaldehyde solution for 15 min. This was followed by rinsing three times with 1x PBS. Thereafter, the nuclei of the A549 cells were stained with DAPI (1 µg/ml). Finally, the cells were rinsed three times with 1x PBS and then mounted, and imaged using an Olympus IX70 fluorescence microscope equipped with a 120 W mercury vapor short arc lamp (X-Cite series 120, EXFO) and appropriate band-pass filters for collecting emission signals of DAPI and urchin-like $GdPO_4{\cdot}H_2O$:5Eu^{3+} nanoparticles.

2.6. Surface functionalization, loading and release of an anti-cancer drug

For the surface functionalization of the nanoparticles, 20 mg of urchin-like $GdPO_4{\cdot}H_2O$:5Eu^{3+} nanoparticles were dispersed in 18 ml of propanol. 3-aminopropyltriethoxysilane (APTES) (120 µl) was then added to the nanoparticle solution and the sample bottle was sealed. The sample bottle was then heated in a beaker of water to 80 °C (in heating mantle) for 24 h with constant stirring (490 rpm). After 24 h, the sample was separated using centrifugation (1,000 rpm for 15 min), washed with ethanol several times, and dried in a room-temperature desiccator for 48 h. The functionalized nanoparticles were dispersed in 10 ml DI water, and 500 µg of DOX was added to the nanoparticle solution. The mixture was incubated under constant rotation for 48 h at room temperature in the dark under ambient conditions. The DOX-loaded sample was collected by centrifugation (10,000 rpm for 30 min) and rinsed three times with DI water. To check the drug-loading efficiency, absorbance at 481 nm were measured after collecting the supernatant solution following centrifugation.

To observe the release efficiency of DOX from the urchin-like $GdPO_4{\cdot}H_2O$:5Eu^{3+} nanoparticles, the drug-loaded nanoparticles were suspended in pH 7.4 PBS (to mimic the physiological pH) and pH 4.5 PBS (to mimic the pH of endosomes) solutions. The fluorescence spectra of the collected supernatants were measured at different time intervals to estimate the efficiency of DOX release.

2.7. Statistical analyses

The CCK-8 assay results were analyzed using one-way ANOVA with the Neumann-Keuls test using GraphPad Prism software (La Jolla, CA, USA). Data are expressed as the mean ± SD of three replicated experiments.

3. Results and discussion

Fig. 1 shows field-emission scanning electron microscopy (FE-SEM) and field-emission transmission electron microscopy (FE-TEM) images of the as-synthesized $Gd(OH)CO_3:Eu^{3+}$ precursor. The low-and high-magnification FE-SEM images (Fig. 1a and b) revealed $Gd(OH)CO_3:Eu^{3+}$ nanospheres with a uniform dispersion. The high-magnification FE-SEM image (Fig. 1b) of $Gd(OH)CO_3:5Eu^{3+}$ shows that the surface of the nanospheres was rough and uniform in size (~60 nm in diameter), which was also confirmed by the TEM and high-magnification TEM images (Fig. 1c and d). Fig. 1e–h presents the FE-SEM and FE-TEM images of the urchin-like $GdPO_4{\cdot}H_2O:5Eu^{3+}$ nanoparticles, synthesized at 180 °C for 1 h under hydrothermal conditions. FE-TEM images of the urchin-like $GdPO_4{\cdot}H_2O:5Eu^{3+}$ nanoparticles as a function of reaction time are presented in Fig. S1. After a reaction time of 1 h, the FE-SEM and FE-TEM images of the $GdPO_4{\cdot}H_2O:5Eu^{3+}$ nanoparticles revealed monodispersed urchin-like nanoparticles with a uniform diameter of approximately 150 nm (Fig. 1e–g), which can be attributed to the accumulation of a large number of nanorods (magnified image of Fig. 1g) with the reaction between $Gd(OH)CO_3:5Eu^{3+}$ nanospheres and the H_3PO_4 precursor due to the Kirkendall effect. The following reactions occurred during the formation of the urchin-like $GdPO_4{\cdot}H_2O:5Eu^{3+}$ nanoparticles:

$$H_3PO_4 + 3H_2O \Rightarrow 3H_3O^+ + PO_4^{3-} \quad (1)$$

$$H_3O^+ + PO_4^{3-} + Gd_{0.95}Eu_{0.05}(OH)CO_3 \Rightarrow Gd_{0.95}Eu_{0.05}PO_4 \cdot H_2O + CO_3 \quad (2)$$

During the reaction, $Gd(OH)CO_3:5Eu^{3+}$ nanospheres acted as both chemical and physical templates. The $Gd(OH)CO_3:5Eu^{3+}$ nanospheres were initially surrounded by H^+ ions because of the dissociation of the weak Arrhenius acid H_3PO_4 into H_3O^+ and PO_4^{3-} in water (see Equations (1) and (2)). Molecules of H_3O^+ diffuse Gd^{3+} ions from the $Gd(OH)CO_3:5Eu^{3+}$ nanospheres via ionization. The diffused $Gd^{3+}(Eu^{3+})$ ions react with PO_4^{3-} and induces the formation of $GdPO_4{\cdot}H_2O:5Eu^{3+}$ nanorods. This diffusion from the outer surface of $Gd(OH)CO_3:5Eu^{3+}$ nanospheres occurs due to the mediation of H_3O^+ and facilitates the reaction with PO_4^{3-} to form $GdPO_4{\cdot}H_2O:5Eu^{3+}$ nanorods on the surfaces of $Gd(OH)CO_3:5Eu^{3+}$ nanospheres, resulting in thinner nanospheres (Fig. S1). With increasing reaction time, the

Quantity of $GdPO_4{\cdot}H_2O:5Eu^{3+}$ nanorods also gradually increased whereby the Kirkendall effect takes place through the outward diffusion of Gd^{3+} ions and diffusion of PO_4^{3-} ions inwards because the diffusion velocity of Gd $^{3+}$ ions exceeds that of PO_4^{3-} ions [7,20]. Within 1 h of reaction, the total process was completed by forming $GdPO_4{\cdot}H_2O:5Eu^{3+}$ nanorod-assembled urchin-like nanoparticles. This is faster than the time reported in previous studies where researchers used $NH_4H_2PO_4$ as the phosphate source [7,21]. Upon further increasing the reaction time, the detachment of the $GdPO_4{\cdot}H_2O:5Eu^{3+}$ nanorods from the urchin-like nanoparticles began. The growth process is shown in Scheme 1. The synthesis results demonstrated that H_3PO_4 accelerated the reaction if the Kirkendall effect occurs during the reaction, as compared to when $NH_4H_2PO_4$ was used.

The elemental composition of the urchin-like $GdPO_4{\cdot}H_2O:5Eu^{3+}$ nanoparticles was verified using energy-dispersive X-ray spectroscopy

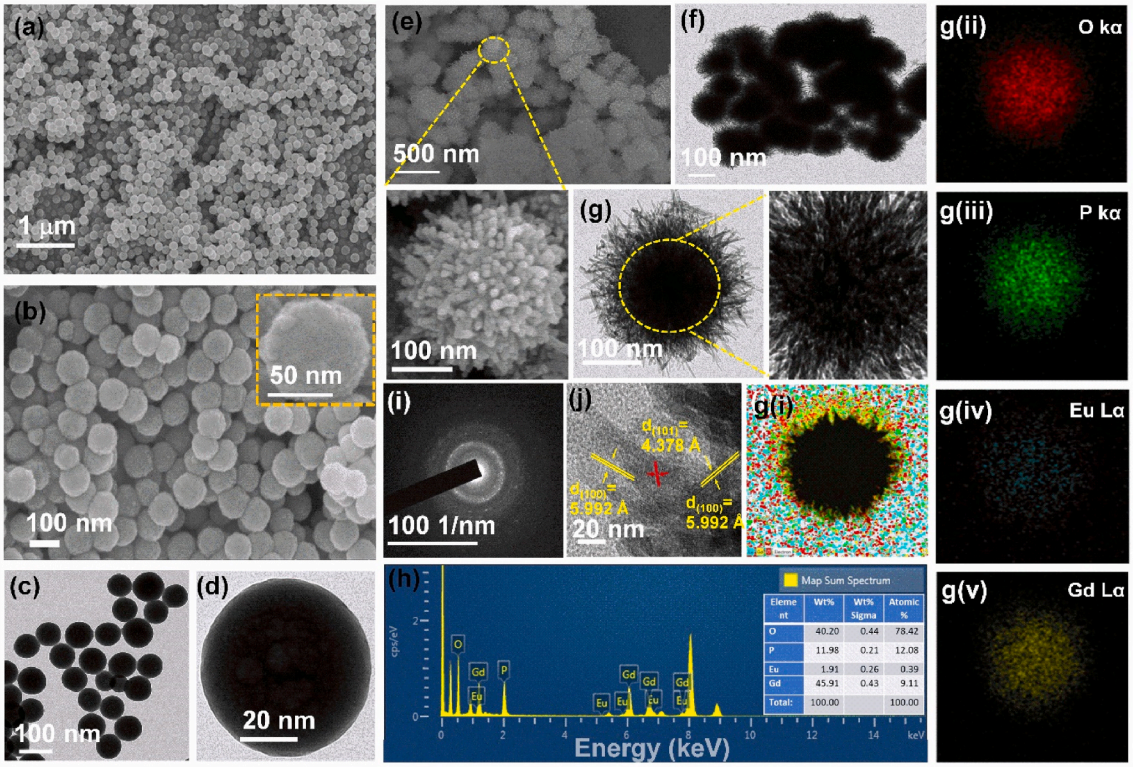

Fig. 1. Morphological images of $Gd(OH)CO_3:5Eu^{3+}$ nanospheres and urchin-like $GdPO_4{\cdot}H_2O:5Eu^{3+}$ nanoparticles: (a and b) FE-SEM and (c and d) FE-TEM images of $Gd(OH)CO_3:5Eu^{3+}$ nanospheres under different magnifications. Low and high magnification, (e) FE-SEM and (f and g) FE-TEM, images of urchin-like $GdPO_4{\cdot}H_2O:5Eu^{3+}$ nanoparticles and corresponding elemental mappings of merged image, O, P, Eu, and Gd elements and EDS spectra are presented in g(i–v) and h respectively. (i and j) Selected area electron diffraction (SAED) pattern and high-resolution transmission electron microscopy (HRTEM) image of an urchin-like $GdPO_4{\cdot}H_2O:5Eu^{3+}$ nanoparticle.

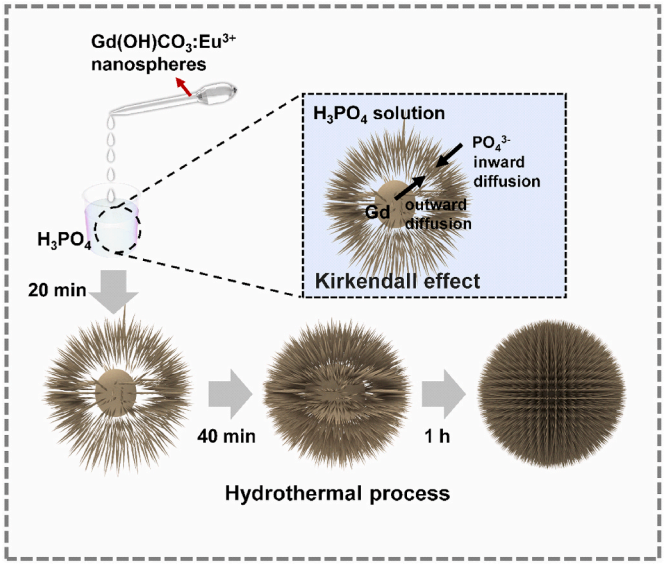

Scheme 1. A representation of the formation of urchin-like $GdPO_4.H_2O:5Eu^{3+}$ nanoparticles.

(EDS) of a single urchin-like $GdPO_4{\cdot}H_2O:5Eu^{3+}$ particle. The resulting spectrum is shown in Fig. 1h and this confirmed the presence of Gd, Eu, P, and O. Most of the Gd and Eu ions were bound to the L shell at 6.51 and 5.85 keV whereas the P and O ions were tied to the K shell at 2.01 and 0.53 keV, respectively. Additionally, elemental mapping (Fig. 1g (i–v) confirmed the uniform distribution of elements within the nanoparticle. In particular, Eu^{3+} ions were scattered homogeneously within the Gd^{3+} sites of the $GdPO_4{\cdot}H_2O$ host lattice (Fig. 1g (iv)), indicating the possibility of good luminescent properties. Fig. 1i shows the selected area electron diffraction (SAED) pattern, revealing strong concentric rings with bright dots on the rings, confirming a nanocrystals–based polycrystalline nature. The corresponding HRTEM image is shown presented in Fig. 1j. The interplanar distance between the vertically developed adjacent lattice fringes was approximately 5.992 Å with the (100) plane and the horizontally developed adjacent fringes was approximately 4.378 Å with the (101) plane.

The X-ray diffraction (XRD) patterns of the as-synthesized $Gd(OH)CO_3:5Eu^{3+}$ precursor and urchin-like $GdPO_4{\cdot}H_2O:5Eu^{3+}$ samples are shown in Fig. 2a. The XRD pattern of $Gd(OH)CO_3:5Eu^{3+}$ did not reveal any sharp diffraction peaks between 10° and 80°, indicating the amorphous nature of the synthesized compound. In contrast, the XRD patterns of $GdPO_4{\cdot}H_2O:5Eu^{3+}$ showed intense and well-resolved diffraction peaks without any impurity phases, consistent with the hexagonal phase of standard JCPDS No. 39–0232 (space group P3121 (152)). The existence of the H_2O phase alongside $GdPO_4$ indicates the enhancement of nanoparticle dispersion in aqueous media compared with oxide phase nanoparticles alone. Therefore, $GdPO_4{\cdot}H_2O:5Eu^{3+}$ nanoparticles are expected to be promising candidates for biomedical applications.

To investigate the functional groups and chemical composition of the $Gd(OH)CO_3:5Eu^{3+}$ nanospheres and urchin-like $GdPO_4{\cdot}H_2O:5Eu^{3+}$ samples, Fourier transform infrared spectroscopy (FTIR) was performed. The FTIR spectrum (Fig. 2b) of $Gd(OH)CO_3:Eu^{3+}$ exhibited the characteristic vibrational bands of O−C−O (asymmetric stretching ν_{as}), with typical doublet absorption bands with band maxima at 1400 and 1508 cm^{-1}. $\pi-CO_3^{2-}$ and $\delta-CO_3^{2-}$ appearing with vibrational peaks were centered at 840 and 699 cm^{-1}, respectively [7,22]. The FTIR spectrum of $GdPO_4{\cdot}H_2O:5Eu^{3+}$ exhibited the vibrational bands of PO_4^{3-} moieties by exhibiting the functional groups of P–O (1080 cm^{-1}) and O−P−O (620 and 536 cm^{-1}) [23,24]. For both $Gd(OH)CO_3:5Eu^{3+}$ and $GdPO_4{\cdot}H_2O:5Eu^{3+}$, the FTIR spectra exhibited O–H stretching vibrations between 2570 and 3740 cm^{-1}. Additionally, $GdPO_4{\cdot}H_2O:5Eu^{3+}$ exhibited O–H bending vibrations at 1626 cm^{-1}, confirming the hydrate phase of $GdPO_4$ urchin-like nanoparticles [23].

The chemical composition and the elemental oxidation states of the $Gd(OH)CO_3:5Eu^{3+}$ and $GdPO_4{\cdot}H_2O:5Eu^{3+}$ samples were verified through XPS measurements (Fig. 2c–f). The XPS survey scans of both

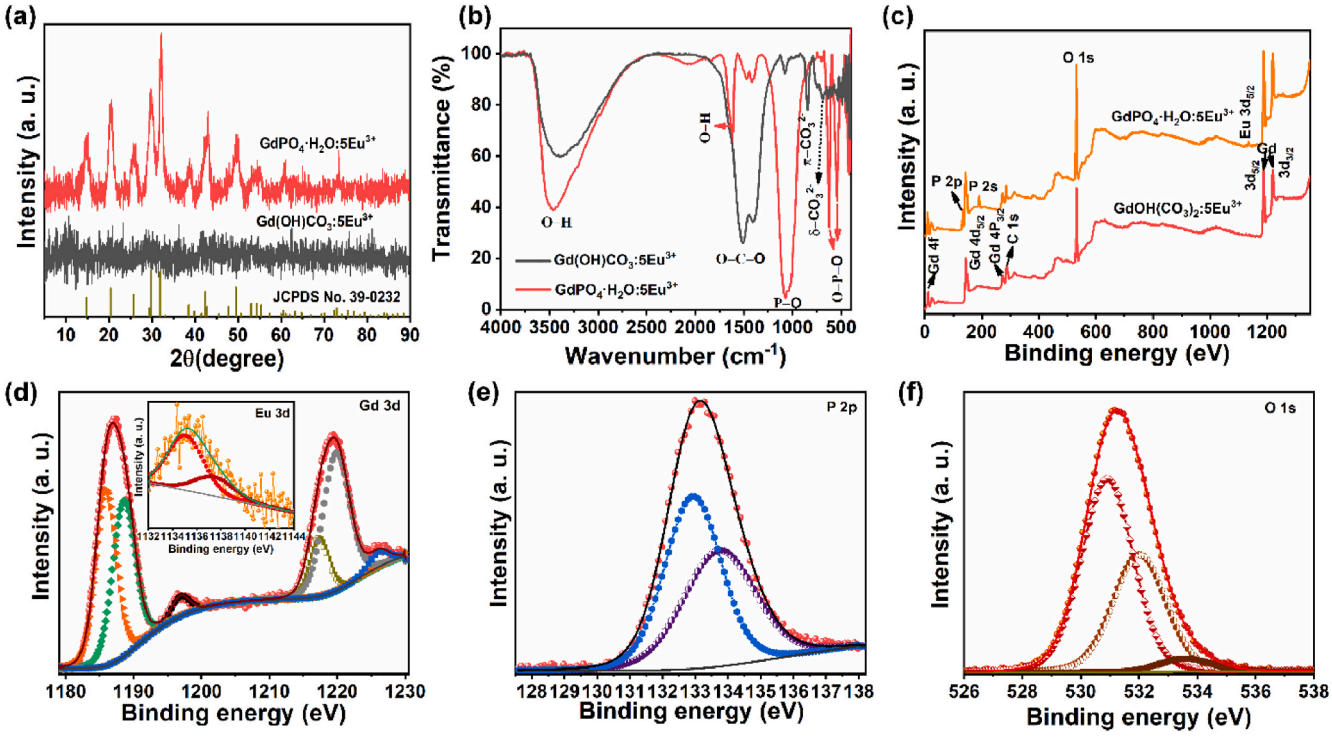

Fig. 2. Structural properties of $Gd(OH)CO_3:5Eu^{3+}$ nanospheres and urchin-like $GdPO_4.H_2O:5Eu^{3+}$ nanoparticles: (a) XRD patterns, (b) FTIR spectra, and (c) XPS spectra and (d–f) high resolution core-level XPS spectra of Gd(Eu), P, and O, respectively.

samples revealed similar Gd peaks with different states, including 4f, $4d_{5/2}$, $4p_{3/2}$, $3d_{5/2}$, and $3d_{3/2}$ at binding energies of 9.5, 142.4, 272.5, 1186.7, and 1219.3, respectively. In addition, $GdPO_4{\cdot}H_2O{:}5Eu^{3+}$ revealed characteristic P bands with 2p and 2s states, located at binding energies of 133.5, and 190.3, respectively. To obtain further insights into the structural properties and ionic states of the rare-earth ions of $GdPO_4{\cdot}H_2O{:}5Eu^{3+}$, core-level high-resolution XPS spectra were measured for Gd, Eu, P, and O ions. Fig. 2d shows the high-resolution core-level Gd3d spectra, where typical doublet $3d_{5/2}$ and $3d_{3/2}$ bands with an energy difference of approximately 32.6 eV. This energy difference corresponds well with those obtained in previous studies that investigated Gd_2O_3, confirming that the Gd^{3+} ions are in the 3+-oxidation state [25–29]. The $3d_{5/2}$ and $3d_{3/2}$ bands were deconvoluted into three peaks. The deconvolved $3d_{5/2}$ peak exhibited $Gd3d_{5/2}$, $Gd_2O_33d_{5/2}$, and satellite peaks with band maxima at 1185.6, 1188.6, and 1187.1 eV, respectively. The deconvolved $3d_{3/2}$ peak exhibited $Gd3d_{3/2}$, $Gd_2O_33d_{3/2}$, and satellite peaks with band maxima at 1217.4, 1219.9 and 1226.5 eV, respectively. The weak satellite peaks that appeared in the Gd3d spectrum could be attributed to energy loss phenomena [26]. The inset of Fig. 2d shows the Eu core-level spectrum and deconvoluted into two peaks, which are ascribed to Eu3d and $Eu3d_{5/2}$, respectively, confirming the doping of Eu^{3+} ions into the Gd^{3+} ion-occupied sites. The P ions in $GdPO_4.H_2O{:}5Eu^{3+}$ exhibited a P2p band (Fig. 2e), which was deonvoluted into two typical peaks, such as $2p_{3/2}$ and $2p_{1/2}$, respectively. Moreover, the O1s spectrum (Fig. 2f) was deconvoluted into three peaks with band maxima at 530.9, 532.1, and 533.7 eV. The O1s peak positioned at 533.7 eV corresponds to the Gd−O species, and the peaks at 530.9 and 532.1 eV can be attributed to the physical and chemical absorption of water molecules and the residual oxygen groups (−OH, C−O, and O−C−O) due to the coordination of Gd−O−Gd [27,29]. The presence of 530.1 and 532.1 eV peaks confirm the formation of $GdPO_4$ with a hydroxide phase [30].

The PL excitation (PLE), emission (PL) spectra, and the corresponding decay curve of the urchin-like $GdPO_4{\cdot}H_2O{:}5Eu^{3+}$ nanoparticles were investigated by monitoring their characteristic emission and excitation wavelengths, respectively. The resulting spectra are displayed in Fig. 3. When the emission wavelength was fixed at 589.5 nm, the PLE spectra exhibited a broad and intense charge transfer excitation band (CTB) between 208 and 267 nm, with a band maximum at 233 nm (Fig. 3a). The CTB appeared due to the charge transfer among the 4f and 2p orbitals of the Eu^{3+} and O^{2-} ions, respectively. However, the position of the CTB was unstable at this particular location. The CTB position relies on the local coordination environment of the host lattice around Eu^{3+} ions along with the covalent bonding of $O^{2-}$and Eu^{3+} ions [31]. The PLE spectra also displayed narrow bands with considerable intensities due to the intra-configurational f-f transitions of Gd^{3+} and Eu^{3+} ions. The intense band observed at 274 nm was recognized as the characteristic peak of Gd^{3+} ions, which can be attributed to the $^8S_{7/2}\rightarrow{}^6I_{7/2}$ transition. The transitions in the longer-energy regions occurred at 311, 318, 361, 379, 394, 415, and 463 nm are ascribed to $^5I_6$, $^5H_4$, $^5D_4$, $^5G_4$, $^5L_6$, $^5D_3$, and $^5D_2$ levels, respectively. Among them, the excitation bands at 233 nm (CTB), 274 nm ($^8S_{7/2}\rightarrow{}^6I_{7/2}$), and 394 nm ($^7F_0\rightarrow{}^5L_6$) are well documented with the emission wavelengths of UV and near-UV chips, demonstrating that the synthesized urchin-like $GdPO_4{\cdot}H_2O{:}5Eu^{3+}$

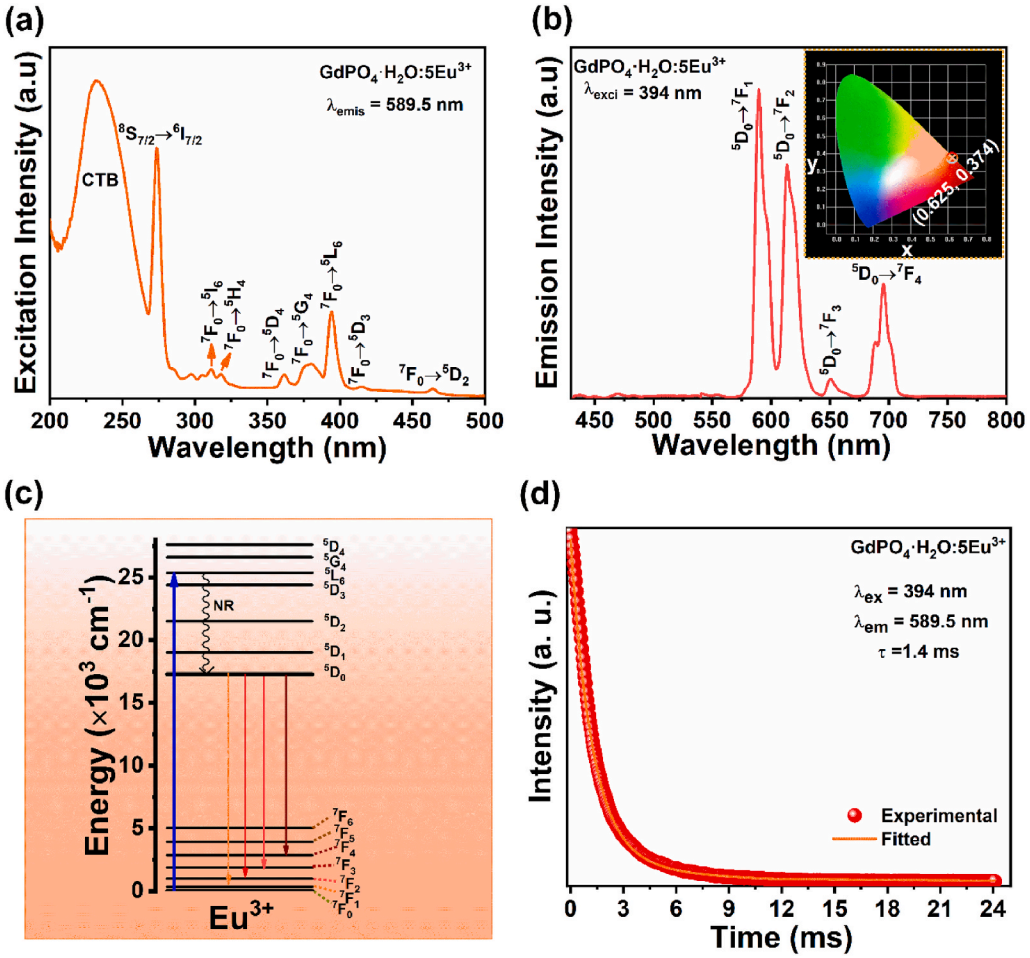

Fig. 3. (a) PL excitation, (b) PL emission (inset shows the CIE diagram for $GdPO_4.H_2O{:}5Eu^{3+}$ urchin-like nanoparticle), (c) energy level diagram, and (d) decay curve of the urchin-like $GdPO_4.H_2O{:}5Eu^{3+}$ nanoparticles.

nanoparticles are suitable for UV and near-UV excitation-based luminescent applications. Fig. 3b shows the PL emission spectrum of urchin-like $GdPO_4{\cdot}H_2O{:}5Eu^{3+}$ nanoparticles under 394 nm excitation. We chose 394 nm wavelength of the excitation spectrum originated from the ground state $^7F_0$ to the higher excitation for this study because all the excitations that appeared in the PLE spectrum exhibited similar emissions, except the intensities. However, for biological applications, near-UV excitation is more feasible compared to UV excitation. The PL spectrum revealed a strong emission band in the reddish-orange region with a band maximum at 589.5 nm, ascribed to the magnetic dipole transition of $^5D_0 \rightarrow {}^7F_1$. The second and third intense emission bands were apparent in the red and far-red regions at 613 ($^5D_0 \rightarrow {}^7F_2$) and 694 nm ($^5D_0 \rightarrow {}^7F_4$), arising from the electric dipole transitions. These were accompanied by moderately intense red emission band at 650 nm ($^5D_0 \rightarrow {}^7F_3$). Furthermore, Eu^{3+} ions occupied the local site symmetry in the $GdPO_4.H_2O$ host lattice, which was estimated by considering the integrated emission intensity ratio of the electric dipole (red emission) and magnetic dipole (orange emission) transitions, also called the asymmetric ratio. According to the Judd–Ofelt theory, Eu^{3+} ions occupy a site without inversion symmetry if the electric dipole transition dominates the magnetic dipole transition (red/orange >1). If the magnetic dipole transition dominates the emission spectrum (red/orange <1), Eu^{3+} ions enter into the inversion symmetry site [32,33]. The red/orange ratio of $GdPO_4{\cdot}H_2O{:}5Eu^{3+}$ was approximately 0.76, demonstrating that the Eu^{3+} ions occupied the Gd^{3+} sites with inversion symmetry. In addition, the Commission International de l'Eclairage chromaticity of $GdPO_4.H_2O{:}5Eu^{3+}$ urchin-like nanoparticles (inset of Fig. 3b) is exhibited in the reddish-orange region with the coordinates of (0.625, 0.374). The PL properties observed in the present study indicated their suitability for bioimaging applications. A schematic of the excitation and emission mechanisms with energy levels is presented in Fig. 3c. Furthermore, the decay profile (Fig. 3d) of the urchin-like $GdPO_4{\cdot}H_2O{:}5Eu^{3+}$ nanoparticles was obtained by employing the excitation and emission wavelengths of 394 nm and 589.5 nm, respectively. The profile obtained in the present study is well-documented to a single exponential function [34,35]:

$$I(t) = I_0 + A\exp\left(\frac{-t}{\tau}\right) \quad (3)$$

where A is a constant and I_0 and $I(t)$ represent the initial luminescence intensity and luminescence intensity at time t, respectively. τ in equation (3) is the decay time, and was found to be ~1.4 ms. Thus, the NUV excitation–based reddish-orange emission from urchin-like $GdPO_4{\cdot}H_2O{:}5Eu^{3+}$ nanoparticles confirms their potential application in diagnosing diseases through bioimaging.

To investigate the feasibility of applying urchin-like $GdPO_4{\cdot}H_2O{:}5Eu^{3+}$ nanoparticles in the biomedical field, bioimaging and drug delivery studies were carried out on A549 lung cancer cells. Fig. 4a–d shows the in vitro fluorescence imaging of the A549 cells, where Fig. 4a shows the control, and Fig. 4b and c shows the confocal microscope images of DAPI alone and $GdPO_4{\cdot}H_2O{:}5Eu^{3+}$ nanoparticles alone, respectively. The merged images of the urchin-like $GdPO_4{\cdot}H_2O{:}5Eu^{3+}$ nanoparticles and DAPI (Fig. 4d) confirmed that the urchin-like nanoparticles exhibited emission from both the cytoplasm and nucleoplasm. The emission of urchin-like $GdPO_4{\cdot}H_2O{:}5Eu^{3+}$ nanoparticles from A549 cells indicated good penetration capability for localizing lung cancer cells. Furthermore, the cytotoxicity of the urchin-like $GdPO_4{\cdot}H_2O{:}5Eu^{3+}$ nanoparticles and the antitumor activity after conjugation of DOX with the urchin-like $GdPO_4{\cdot}H_2O{:}5Eu^{3+}$ nanoparticles ($GdPO_4{\cdot}H_2O{:}5Eu^{3+}$@DOX) were verified by treating the

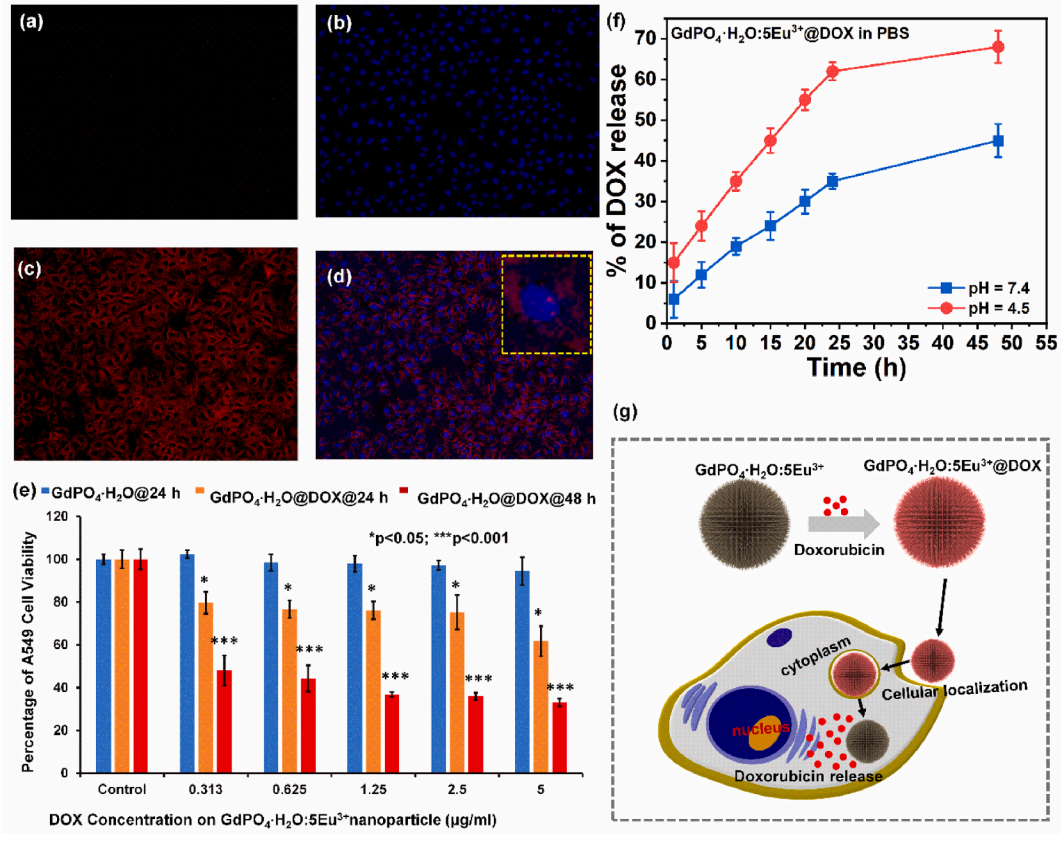

Fig. 4. Confocal fluorescence microscope images of the A549 cell (a) control, (b) after staining with DAPI, (c) after staining with $GdPO_4{\cdot}H_2O{:}5Eu^{3+}$, and (d) merged image (inset shows the magnified merged image of the A549 cell). (e) Cell viability confirmation using cytotoxicity assay. (f) DOX releasing capacity of the urchin-like $GdPO_4{\cdot}H_2O{:}5Eu^{3+}$ nanoparticles at different intervals of times under different pH values. (g) Schematic for the cellular localization and DOX releasing of urchin-like $GdPO_4{\cdot}H_2O{:}5Eu^{3+}$ nanoparticles.

A549 cells. The DOX loading percentage on the urchin-like $GdPO_4{\cdot}H_2O{:}5Eu^{3+}$ nanoparticles was estimated as approximately ~95%. The DOX loading occurred with the help of active electrostatic interactions between the surface amine groups due to the functionalization of $GdPO_4{\cdot}H_2O{:}5Eu^{3+}$ nanoparticles with APTES and carbonyl groups of the DOX molecules under neutral conditions [36]. This was further confirmed by measuring the zeta potentials (Fig. S2), which were 15.91 mV and −11.76 mV for $GdPO_4{\cdot}H_2O{:}5Eu^{3+}$ and $GdPO_4{\cdot}H_2O{:}5Eu^{3+}$@DOX, respectively. Different concentrations of $GdPO_4{\cdot}H_2O$ and $GdPO_4{\cdot}H_2O{:}5Eu^{3+}$@DOX were used to examine the cell viability and antitumor activity.

The obtained results are presented in Fig. 4e. It can be seen that, urchin-like $GdPO_4{\cdot}H_2O{:}5Eu^{3+}$ nanoparticles did not have any significant impact on cell viability; however, $GdPO_4{\cdot}H_2O{:}5Eu^{3+}$@DOX had a significant impact on A549 cells with respect to the applied concentration (Fig. 4e). With an increase in $GdPO_4{\cdot}H_2O{:}5Eu^{3+}$@DOX concentration, the cell viability decreased. After 24 h of treatment with 0.313 μg/ml and 5 μg/ml DOX on the $GdPO_4{\cdot}H_2O{:}5Eu^{3+}$ nanoparticles, the survival rates of A549 cells were approximately 79.69% and 61.75% ($P<0.05$), respectively. After 48 h, these proportions reduced to about 47.96% and 33.09% ($P<0.001$), suggesting that the urchin-like $GdPO_4{\cdot}H_2O{:}5Eu^{3+}$ nanoparticles were effective in releasing DOX in the A549 cells. The half-maximal inhibitory concentration of DOX (0.313 μg) after loading on the urchin-like $GdPO_4{\cdot}H_2O{:}5Eu^{3+}$ nanoparticles, was observed for A549 cells after 48 h of treatment. Moreover, the DOX releasing capacity from the urchin-like $GdPO_4{\cdot}H_2O{:}5Eu^{3+}$ nanoparticles was determined at different intervals of time and at different pH values of pH 7.4 and pH 4.5. The observed values are presented in Fig. 4f. Furthermore, a higher releasing efficiency of DOX from the $GdPO_4{\cdot}H_2O{:}5Eu^{3+}$ nanoparticles was observed in acidic conditions compared to the neutral conditions (Fig. 4f), indicating that the electrostatic interactions between the hydroxyl groups of $GdPO_4{\cdot}H_2O{:}5Eu^{3+}$ and amine groups of DOX was weaker under acidic conditions. Therefore, urchin-like $GdPO_4{\cdot}H_2O{:}5Eu^{3+}$@DOX nanoparticles exhibited a better release efficiency in tumors (acidic) than blood (pH = 7.4). The hypothetical mechanism of cellular internalization and drug release from urchin-like $GdPO_4{\cdot}H_2O{:}5Eu^{3+}$@DOX nanoparticles is presented in Fig. 4g. Thus, the obtained results indicate that urchin-like $GdPO_4{\cdot}H_2O{:}5Eu^{3+}$ nanoparticles show great promise as potential materials for multifunctional biomedical applications.

4. Conclusions

In this study, an effective and energy-saving hydrothermal synthesis of Kirkendall effect-induced urchin-like $GdPO_4{\cdot}H_2O{:}5Eu^{3+}$ nanoparticles was reported. The spherical and urchin shapes were confirmed by FE-SEM and FE-TEM images. The $Gd(OH)CO_3{:}5Eu^{3+}$ nanospheres, with sizes of about 60 nm acted as the Gd^{3+} source and sacrificing template, while H_3PO_4 as the phosphate source accelerated the rate of reaction to form urchin-like $GdPO_4{\cdot}H_2O{:}5Eu^{3+}$ nanoparticles. The XRD patterns revealed that the synthesized $GdPO_4{\cdot}H_2O{:}5Eu^{3+}$ nanoparticles had a pure hexagonal phase. The FTIR spectrum verified the H_2O phase of the GdPO4:$5Eu^{3+}$ nanoparticles, and the EDS and XPS spectra confirmed the doping of Eu^{3+} ions at the Gd sites of $GdPO_4{\cdot}H_2O{:}5Eu^{3+}$. The PL spectra confirmed the inversion symmetry of Eu^{3+} ions in the $GdPO_4{\cdot}H_2O$ host lattice, revealing reddish-orange emissions under near-UV excitation. The confocal microscope images validated the effective penetration capability of the urchin-like $GdPO_4{\cdot}H_2O{:}5Eu^{3+}$ nanoparticles in A549 cells, exhibiting luminescence from both the cytoplasm and nucleoplasm. The viability of A549 cells decreased significantly after treatment with DOX-conjugated urchin-like $GdPO_4{\cdot}H_2O{:}5Eu^{3+}$ nanoparticles. The results suggest that the synthesized urchin-like $GdPO_4{\cdot}H_2O{:}5Eu^{3+}$ nanoparticles are promising materials for multifunctional biomedical applications.

Declaration of competing interest

The authors declare that they have no known competing financial interests or personal relationships that could have appeared to influence the work reported in this paper.

Acknowledgements

This work was supported by the National Research Foundation of Korea (NRF) grants funded by the Korean government (MSIT) (2020R1I1A1A01072635 and 2021R1A5A6002853).

Appendix A. Supplementary data

Supplementary data to this article can be found online at https://doi.org/10.1016/j.ceramint.2022.05.086.

References

[1] S. Bayda, M. Adeel, T. Tuccinardi, M. Cordani, F. Rizzolio, The history of nanoscience and nanotechnology: from chemical-physical applications to nanomedicine, Molecules 25 (2019) 112.
[2] S. Parvanian, S.M. Mostafavi, M. Aghashiri, Multifunctional nanoparticle developments in cancer diagnosis and treatment, Sensing and Bio-Sensing Research 13 (2017) 81–87.
[3] R. Jadia, C. Scandore, P. Rai, Nanoparticles for effective combination therapy of cancer, Int. J. Nanotechnol. Nanomed. 1 (2016) 1–22.
[4] Pushpendra, I. Suryawanshi, S. Srinidhi, S. Singh, R. Kalia, R.K. Kunchala, S. L. Mudavath, B.S. Naidu, Downshifting and upconversion dual mode emission from lanthanide doped $GdPO_4$ nanorods for unclonable anti-counterfeiting, Mater. Today Commun. 26 (2021), 102144.
[5] Y. Wang, H. Zhang, S. Qu, C. Su, Downconversion and upconversion emissions of $GdPO_4{:}Yb^{3+}/Tb^{3+}$ and its potential applications in solar cells, J. Alloys Compd. 677 (2016) 266–270.
[6] Y. Gao, Y. Qiu, X. Wang, Y. Bi, G. Zhao, F. Ding, Y. Sun, Z. Xu, Large-scale synthesis and luminescence of $GdPO_4$ hollow microspheres, RSC Adv. 8 (2018) 21857–21862.
[7] Z. Xu, Y. Cao, C. Li, P.a. Ma, X. Zhai, S. Huang, X. Kang, M. Shang, D. Yang, Y. Dai, J. Lin, Urchin-like $GdPO_4$ and $GdPO_4{:}Eu^{3+}$ hollow spheres – hydrothermal synthesis, luminescence and drug-delivery properties, J. Mater. Chem. 21 (2011) 3686–3694.
[8] F. Zheng, W. Xiong, S. Sun, P. Zhang, J.J. Zhu, Recent advances in drug release monitoring, Nanophotonics 8 (2019) 391–413.
[9] A. Fatima, M.W. Ahmad, A.K.A. Al Saidi, A. Choudhury, Y. Chang, G.H. Lee, Recent advances in gadolinium based contrast agents for bioimaging applications, Nanomaterials (Basel, Switzerland) 11 (2021) 2449.
[10] J. Zhao, J. Chen, S. Ma, Q. Liu, L. Huang, X. Chen, K. Lou, W. Wang, Recent developments in multimodality fluorescence imaging probes, Acta Pharm. Sin. B B 8 (2018) 320–338.
[11] M. Chen, R. Dong, J. Zhang, H. Tang, Q. Li, H. Shao, X. Jiang, Nanoscale metal–organic frameworks that are both fluorescent and hollow for self-indicating drug delivery, ACS Appl. Mater. Interfaces 13 (2021) 18554–18562.
[12] G.S.R. Raju, E. Pavitra, H. Lee, G. Nagaraju, R. Baskaran, S.G. Yang, C.H. Kwak, G. P. Nagaraju, Y.S. Huh, Y.-K. Han, Pre-ouzo effect derived fergusonite gadolinium ortho-niobate mesoporous nanospheroids for multimodal bioimaging and photodynamic therapy, Appl. Surf. Sci. 505 (2020), 144584.
[13] S.F. Soares, T. Fernandes, A.L. Daniel-da-Silva, T. Trindade, The controlled synthesis of complex hollow nanostructures and prospective applications, Proc. R. Soc. A 475 (2019), 20180677.
[14] G. Prieto, H. Tüysüz, N. Duyckaerts, J. Knossalla, G.-H. Wang, F. Schüth, Hollow nano- and microstructures as catalysts, Chem. Rev. 116 (2016) 14056–14119.
[15] X. Wang, J. Feng, Y. Bai, Q. Zhang, Y. Yin, Synthesis, properties, and applications of hollow micro-/nanostructures, Chem. Rev. 116 (2016) 10983–11060.
[16] H.J. Fan, U. Gösele, M. Zacharias, Formation of nanotubes and hollow nanoparticles based on kirkendall and diffusion processes: a review, Small 3 (2007) 1660–1671.
[17] L. Zhang, M. Yin, H. You, M. Yang, Y. Song, Y. Huang, Multifunctional $GdPO_4{:}Eu^{3+}$ hollow spheres: synthesis and magnetic and luminescent properties, Inorg. Chem. 50 (2011) 10608–10613.
[18] Z. Li, Z. Liu, M. Yin, X. Yang, J. Ren, X. Qu, Combination delivery of antigens and cpg by lanthanides-based core-shell nanoparticles for enhanced immune response and dual-mode imaging, Adv. Healthcare Mater. 2 (2013) 1309–1313.
[19] E. Pavitra, G. Seeta Rama Raju, G.P. Nagaraju, G. Nagaraju, Y.-K. Han, Y.S. Huh, J. S. Yu, TPAOH assisted size-tunable Gd_2O_3@mSi core–shell nanostructures for multifunctional biomedical applications, Chem. Commun. 54 (2018) 747–750.
[20] Y. Yu, X. Yin, A. Kvit, X. Wang, Evolution of hollow TiO_2 nanostructures via the kirkendall effect driven by cation exchange with enhanced photoelectrochemical performance, Nano Lett. 14 (2014) 2528–2535.

[21] Z. Yi, W. Lu, C. Qian, T. Zeng, L. Yin, H. Wang, L. Rao, H. Liu, S. Zeng, Urchin-like Ce/Tb co-doped $GdPO_4$ hollow spheres for in vivo luminescence/X-ray bioimaging and drug delivery, Biomater. Sci. 2 (2014) 1404–1411.

[22] G.S.R. Raju, E. Pavitra, J.S. Yu, Facile template free synthesis of $Gd_2O(CO_3)_2{\cdot}H_2O$ chrysanthemum-like nanoflowers and luminescence properties of corresponding Gd_2O_3:RE^{3+} spheres, Dalton Trans. 42 (2013) 11400–11410.

[23] X. Zou, L. He, D. Tan, F. Lei, N. Jiang, Q. Zheng, D. Lin, C. Xu, Y. Liu, Anneal-induced transformation of phase structure, morphology and luminescence of $GdPO_4$:Sm^{3+} nanomaterials synthesized by a hydrothermal method, Dalton Trans. 46 (2017) 2948–2956.

[24] M. Yang, H. You, G. Jia, Y. Huang, Y. Song, Y. Zheng, K. Liu, L. Zhang, Selective synthesis of hexagonal and monoclinic $LaPO_4$:Eu^{3+} nanorods by a hydrothermal method, J. Cryst. Growth 311 (2009) 4753–4758.

[25] D. Raiser, J.P. Deville, Study of XPS photoemission of some gadolinium compounds, J. Electron. Spectrosc. Relat. Phenom. 57 (1991) 91–97.

[26] A.P. Milanov, T. Toader, H. Parala, D. Barreca, A. Gasparotto, C. Bock, H.-W. Becker, D.K. Ngwashi, R. Cross, S. Paul, U. Kunze, R.A. Fischer, A. Devi, Lanthanide oxide thin films by metalorganic chemical vapor deposition employing volatile guanidinate precursors, Chem. Mater. 21 (2009) 5443–5455.

[27] G. Vijayaprasath, I. Habibulla, V. Dharuman, S. Balasubramanian, R. Ganesan, Fabrication of Gd_2O_3 nanosheet-modified glassy carbon electrode for nonenzymatic highly selective electrochemical detection of vitamin B_2, ACS Omega 5 (2020) 17892–17899.

[28] S. Majeed, S.A. Shivashankar, Rapid, microwave-assisted synthesis of Gd_2O_3 and Eu:Gd_2O_3 nanocrystals: characterization, magnetic, optical and biological studies, J. Mater. Chem. B 2 (2014) 5585–5593.

[29] M. Ahrén, L. Selegård, F. Söderlind, M. Linares, J. Kauczor, P. Norman, P.-O. Käll, K. Uvdal, A simple polyol-free synthesis route to Gd_2O_3 nanoparticles for MRI applications: an experimental and theoretical study, J. Nanopart. Res. 14 (2012) 1006.

[30] H. Jiang, Y. Guo, T. Wang, P.-L. Zhu, S. Yu, Y. Yu, X.-Z. Fu, R. Sun, C.-P. Wong, Electrochemical fabrication of Ni(OH)2/Ni 3D porous composite films as integrated capacitive electrodes, RSC Adv. 5 (2015) 12931–12936.

[31] D. Kim, J.R. Jeong, Y. Jang, J.-S. Bae, I. Chung, R. Liang, D.-K. Seo, S.-J. Kim, J.-C. Park, Self-emitting blue and red EuOX (X = F, Cl, Br, I) materials: band structure, charge transfer energy, and emission energy, Phys. Chem. Chem. Phys. 21 (2019) 1737–1749.

[32] B. Qian, Y. Wang, Q. Zhao, X. Zhou, H. Zou, Y. Song, K. Zheng, Y. Sheng, Preparation and luminescence properties of Eu^{3+} incorporated in $CaCO_3$ nanocrystals with multiple sites, J. Lumin. 239 (2021), 118344.

[33] J. Zhou, L. Xie, J. Zhong, H. Liang, J. Zhang, M. Wu, Site occupancy and luminescence properties of Eu^{3+} in double salt silicate $Na_3LuSi_3O_9$, Opt. Mater. Express 8 (2018) 736–743.

[34] M. Liu, B. Shen, K. Wang, J. Zhong, D. Chen, Highly efficient red-emitting Ca_2YSbO_6:Eu^{3+} double perovskite phosphors for warm WLEDs, RSC Adv. 9 (2019) 20742–20748.

[35] L. Zhou, P. Du, L. Li, Facile modulation the sensitivity of Eu^{2+}/Eu^{3+}-coactivated Li_2CaSiO_4 phosphors through adjusting spatial mode and doping concentration, Sci. Rep. 10 (2020) 20180.

[36] M. Nerantzaki, A. Michel, E. Briot, J.M. Siaugue, C. Ménager, C. Wilhelm, N. Griffete, Controlled drug delivery for cancer cell treatment via magnetic doxorubicin imprinted silica nanoparticles, Chem. Commun. 56 (2020) 10255–10258.